Modeling settling tanks for water treatment using computational fluid dynamics

Anastasios Stamou and Anthoula Gkesouli

ABSTRACT

A computational fluid dynamics model is presented for the calculation of the flow, suspended solids, and tracer concentration fields in the settling tanks of the water treatment plant of Aharnes, an important component of the water supply system of the greater area of Athens, Greece. The model is applied to investigate the expected negative effect of the wind on the hydraulic and settling performance of the tanks and to evaluate the improvement resulting from the installation of one and two baffles; the wind is modeled using a simple and very conservative approach that involves the setting of a constant horizontal flow velocity on the free surface. The model is calibrated and verified with field turbidity measurements. Calculations show that the effect of wind on the flow field and the hydraulic efficiency is strong, with the creation of massive re-circulation areas with intense mixing and high short circuiting; however, the effect of wind on the settling performance of the tanks is not pronounced. The removal efficiency of the tanks, which is 72.48% in calm conditions, is reduced to 68.07% for windy conditions; moreover, it increases to 70.00 and 71.04%, when one or two baffles are installed, respectively.

Key words | baffles, computational fluid dynamics (CFD), flow through curves (FTCs), settling tanks, wind effect

Anastasios Stamou (corresponding author)
Anthoula Gkesouli
School of Civil Engineering,
National Technical University of Athens,
5 Heroon Polytechniou Str.,
15780 Athens,
Greece
E-mail: *stamou@central.ntua.gr*

INTRODUCTION

Sedimentation is one of the most important treatment processes in conventional water treatment plants (WTPs); a significant percentage of suspended solids (SS), which is formed by the aggregation of particles of the untreated water with flocculants in the upstream coagulation units, settles by gravity and therefore influences the degree of treatment of the downstream units of filtration and disinfection and subsequently the efficiency of the plant. Sedimentation is performed in circular or rectangular settling tanks; the determination of the removal efficiency of these tanks has been the subject of numerous theoretical and experimental studies. In the early to mid-20th century, Hazen (1904) and Camp (1946) presented the classical theory of ideal settling that is based on the concept of overflow rate (OR). According to this theory, sedimentation occurs in an ideal tank, in which the flow is steady, horizontal and free from inlet and outlet disturbances (this flow field is usually called plug flow (PF)), and the solids settle freely as in quiescent conditions (without any re-entrainment or flocculation); the OR concept is still applied in the design of settling tanks.

In real tanks, however, the flow field is usually 3-D and complex being characterized by re-circulation regions (Stamou *et al.* 1989, 2000) that enhance mixing and influence the sedimentation of SS via their flocculation (Lyn *et al.* 1992), breakup or re-entrainment, which depend on their physical characteristics, such as particle size, density and settling velocity (Stamou *et al.* 2009). Owing to its importance, the determination of the hydrodynamic characteristics of settling tanks has also been the subject of numerous studies. It can be achieved: (1) experimentally, via the performance of velocity measurements; (2) numerically, with computational fluid dynamics (CFD) models; and (3) via the experimental or numerical derivation of flow through curves (FTCs).

doi: 10.2166/hydro.2015.069

The performance of flow velocity measurements, usually via Laser Doppler velocimetry (Shiono & Teixeira 2000), is a costly and time-consuming task; moreover, it can be applied only in existing tanks for upgrading and modification purposes, and not in tanks that are in the stage of design.

CFD models have been applied in various chemical/water engineering problems, such as in membrane reactors (Ghidossi *et al.* 2006), trickle-bed reactors (Souadnia *et al.* 2005), chlorination tanks (Falconer & Liu 1987; Shiono & Teixeira 2000; Stamou 2002), oxidation tanks (Stamou 1993), industrial multi-staged stirred vessels (Alliet-Gaubert *et al.* 2006), column separations (Egorov *et al.* 2005), and flocculation tanks (Bridgeman *et al.* 2010). Dufresne *et al.* (2009) stated that even though the measurements are probably the best indicator for understanding the flow and pollutant behavior in a tank, they cannot be carried out before its construction and only CFD models can be applied a priori. Matko *et al.* (1996) reviewed the numerical modeling techniques that are applied to sedimentation tanks in wastewater treatment; they pointed out that CFD models are capable of predicting the flow pattern and SS concentration distributions within the tanks and of finding the relationship between the tank hydraulics and process performance. Liu & Garcia (2007) developed a 3-D multiphase numerical model for the design of the primary settling tank at the Calumet water reclamation plant at Chicago implementing the Flux-Drift model, which is derived from the two-fluid model (Brennan 2001), to describe the behavior of the solid-water mixture, in which the solid volume fraction at the inlet was equal to 10^{-3} or 1,000 mg/L. Owing to the relatively high inlet solids concentration Liu & Garcia (2007) also modeled: (i) hindered settling using an empirical exponential relationship between the settling velocity and the local solids concentration (see also Stamou *et al.* 2009); (ii) coagulation following the approach of Lyn *et al.* (1992); and (iii) flow of settled sludge (blanket) as Bingham plastic with parameters estimated from experiments. Goula *et al.* (2008) presented a CFD methodology for the design of sedimentation tanks in potable water treatment. CFD models have been extensively used to assess the effect of various parameters and alternative modifications on the hydraulic and removal efficiency of settling tanks, including inlet configurations with or without the installation of baffles (Goula *et al.* 2008) and use of lamellas (Okoth *et al.* 2008). Prior to its use, a CFD model must be validated. The validity of CFD models in settling tanks can be checked by comparing the model's results with experimental data (Stamou 2007), which include flow velocity distributions, streamline patterns, size of recirculation regions, SS concentration profiles and/or removal efficiencies.

FTCs can be derived experimentally using a simple tracer technique (Stamou & Noutsopoulos 1994). A mass of tracer is injected at the inlet of the tank instantaneously and the plot of tracer concentration at the outlet vs. time is the FTC. The FTC is essentially the probability density function (pdf) of the detention times in the tank (Stamou & Noutsopoulos 1994); its shape and statistical characteristics provide information regarding the main convective and diffusive (dispersion) characteristics of the flow. Therefore, it can be used for assessing the hydraulic performance of different geometrical configurations in tanks or reactors, including settling tanks.

It is generally recognized that sedimentation tanks are sensitive to wind effects (Asgharzadeh *et al.* 2012); however, the latter are usually neglected and there are only a few relevant studies in the literature. Sivakumar & Lowe (1990) investigated the effect of wind on the removal efficiency of a rectangular settling tank using a 2-D model that involves the k-ϵ turbulence model (Rodi 2000) and observed that with increasing wind speed, the re-circulation region in the tank becomes more extended leading to intense mixing and uniform distribution of the SS. Moreover, they concluded that the wind has a detrimental effect on the distribution of SS and the removal efficiency decreases with increasing wind speed with counter current wind speed being more significant. Khezri *et al.* (2012) performed an experimental study in a pilot sedimentation tank and concluded that: (i) the actual efficiency of the tank (61.24%) decreases with co-current wind speeds of 4.5, 5.5, and 7.0 m/s to 50.01, 46.04, and 45.03%, respectively; (ii) for counter current wind speed equal to 2.5 m/s the efficiency increases to 65.00% due to the increase of solids retention time; and (iii) when the counter current wind speed increases to 3.5 and 5.0 m/s, the efficiency decreases to 55.07 and 47.00%, respectively, due to re-suspension of solids.

In the present work, a CFD model is presented that is based on the commercial code CFX (2013) to calculate the flow field, the SS concentration field, and the FTC in the settling tanks of the WTP of Aharnes in Athens, Greece. The model is applied to investigate the expected negative effect of the wind on the hydrodynamic and settling performance of the tanks and to evaluate the improvement resulting from the installation of one and two baffles in the tank.

THE CHARACTERISTICS OF THE SETTLING TANKS AND THE PRACTICAL PROBLEM

The WTP and the settling tanks in Aharnes

Drinking water is supplied to the city of Athens from four WTPs in the areas of Galatsi, Aharnes, Polydendri, and Aspropyrgos, which have a total capacity of 1.9×10^6 m^3/d. The treatment of raw water in these plants involves coagulation, sedimentation, sand filtration, and chlorination. The WTP in Aharnes (WTPA), which provides water to the areas of Athens with high altitude, consists of two hydraulically independent treatment lines: the 'old' and the 'new' line. Settling in the old line is performed in 16 similar rectangular settling tanks that are shown in Figure 1. The total flow rate to the settling tanks ranges from 4.0 to 5.0 m^3/s.

The top view of each tank is shown in Figure 2(a); the tank has a length equal to $L = 73.2$ m, width equal to $w = 14.4$ m, and an average water depth equal to $H = 3.5$ m. Water from flocculation tanks enters into the settling tanks via four inlet openings, which are located near the bottom of the tanks, and exits via a series of V-notch weirs installed at three outlet channels. The flow rate to each tank (Q) ranges from 0.25 to 0.31 m^3/s, which corresponds to OR ranging from 0.85 to 1.07 m/h and theoretical detention times (T) from 4.1 to 3.3 h.

Figure 1 | The settling tanks of the WTPA (obtained from http://www.google.de/intl/de/earth/).

The practical problem and the proposed method of solution

The settling tanks of the WTPA occasionally experience the effect of strong northerly winds with maximum velocities of the order of 10.0 m/s in the direction x that is parallel to the side walls of the tanks (see Figure 1), i.e., toward the outlet channels. During these windy conditions, the personnel of the WTPA observed the development of waves on the water surface of the tanks and very high turbidity, especially in the first half of the tanks; however, the turbidity values at the effluent were always less than 2.0–2.5 NTU. Moreover, it should be noted that the water quality of the effluent is excellent. We have been asked by the Athens Water Supply and Sewerage Company (EYDAP SA): (i) to determine quantitatively the expected detrimental effect of these winds on the efficiency of the tanks; and (ii) to propose relatively simple and inexpensive measures to deal with this effect. Based on our experience in similar situations (Stamou 2002), we suggested the use of baffles that are an inexpensive and simple means to reduce short circuiting and improve the hydraulic efficiency of the tanks. Initially, we proposed to examine the use of one and two baffles at the locations that are shown in Figure 2(b) and 2(c), respectively. The first baffle is located at $x = L/2 = 36.6$ m and the second at $x = L/4 = 18.3$ m. The thickness of the baffles was 0.10 m and their lower edge was 0.50 m from the surface, i.e., their submergence was equal to 14%.

Subsequently, we performed calculations for four scenarios: (a) calm conditions, without wind (n-W); (b) windy conditions (W); (c) windy conditions and one baffle (W-1B); and (d) windy conditions and two baffles (W-2B). All calculations were performed for three OR values equal to 0.85, 0.96, and 1.07 m/h.

It is noted that during the investigation period, the mechanical scrapers of the settling tanks were out of operation due to technical reasons and the removal of sludge

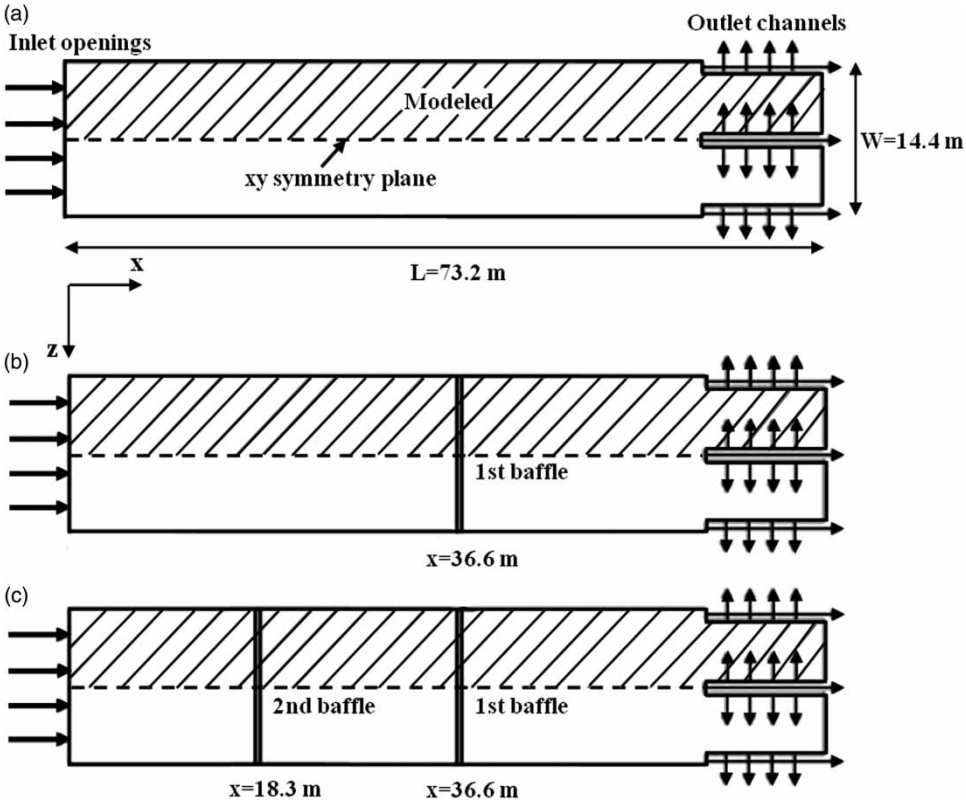

Figure 2 | Top view of the tank: (a) initial, (b) with one baffle, (c) with two baffles.

was performed periodically (typically every 2 months) via portable pumps. Subsequently, the solids that settled were accumulated in the tank forming a sludge blanket, the height of which has been progressively increasing with time.

EQUATIONS OF THE MODEL

Algebraic slip model

We use the algebraic slip model that is virtually a simplified variation of the drift flux model by Ishii (1975), which assumes a continuous medium-mixture (i.e., the water in the settling tanks) with a dispersed phase component (i.e., the SS). This mixture behaves as a single fluid and generally its density (ρ_m) can be affected by the presence of solids at any point of the mixture. In the present work, the SS (with density $\rho_s = 2{,}730\ \mathrm{kg/m^3}$) are divided into four ($n = 1, 4$) classes of different mass fractions ($Y_{s,n}$), volume fractions ($r_{s,n} = Y_{s,n}\rho_m/\rho_s$), diameters ($d_{s,n}$), and settling velocities ($V_{s,n}$); each class of solids is modeled by a mass balance equation, which allows a relative movement (phase slip, i.e., settling) between the solids and the continuous medium (water).

Flow field equations

The 3-D flow field in the settling tanks is governed by the bulk continuity and momentum, Equations (1) and (2), respectively, which are derived by summing the corresponding equations over both phases and classes (ANSYS-CFX 2013).

$$\frac{\partial \rho_m}{\partial t} + \frac{\partial (\rho_m U_m^i)}{\partial x^i} = 0 \tag{1}$$

$$\frac{\partial (\rho_m U_m^i)}{\partial t} + \frac{\partial \left(\rho_m U_m^j U_m^i\right)}{\partial x^j} = -\frac{\partial P}{\partial x^i} + \frac{\partial (\tau_m^{ij} + \tau_{Tm}^{ij} + \tau_{Dm}^{ij})}{\partial x^j} + g^i \rho_m \tag{2}$$

where t is the time, x^i is the Cartesian coordinate in the i-direction, U_m^i is the mixture flow velocity in the i-direction, P is the pressure, g^i is the acceleration of gravity, and τ_m^{ij}, τ_{Tm}^{ij}, and τ_{Dm}^{ij} are the viscous, turbulent, and apparent diffusion stresses, respectively.

Using the subscripts m, w, and s,n to denote quantities for the mixture, water phase, and class of solids, respectively, we write the equations for the properties of the mixture as follows:

$$\rho_m = r_w\rho_w + \rho_s\sum_{n=1}^{4} r_{s,n} \tag{3}$$

$$U_m^i = \frac{1}{\rho_m}\left[r_w\rho_w U_w^i + \rho_s\sum_{n=1}^{4} r_{s,n}U_{s,n}^i\right] \tag{4}$$

$$\begin{aligned}\tau_m^{ij} &= r_w\tau_w^{ij} + \sum_{n=1}^{4} r_{s,n}\tau_{s,n}^{ij}\\ &= r_w\mu_w\left(\frac{\partial U_w^i}{\partial x^j} + \frac{\partial U_w^j}{\partial x^i}\right) + \sum_{n=1}^{4} r_{s,n}\tau_{s,n}^{ij}\end{aligned} \tag{5}$$

$$\tau_{Tm}^{ij} = \mu_{t_m}\left(\frac{\partial U_m^i}{\partial x^j} + \frac{\partial U_m^j}{\partial x^i}\right) - \frac{2}{3}\delta^{ij}\rho_m k_m \tag{6}$$

$$\tau_{Dm}^{ij} = -\rho_w r_w U_{Dw}^i U_w^j - \rho_s\sum_{n=1}^{4} r_{s,n}U_{Ds,n}^i U_{s,n}^j \tag{7}$$

In Equation (7) we denote with U_{Dw}^i and $U_{Ds,n}^i$ the drift velocities for the water and the solids, respectively, i.e., $U_{Dw}^i = U_w^i - U_m^i$ and $U_{Ds,n}^i = U_{s,n}^i - U_m^i$. In Equation (6) we apply the Bussinesq approximation for the calculation of the Reynolds (turbulent) stresses, where μ_{tm} is the eddy viscosity of the mixture, δ^{ij} is the Kronecker delta ($\delta^{ij} = 1$ for $i = j$ and $\delta^{ij} = 0$ for $i \neq j$), and k_m is the turbulent kinetic energy; the distribution of μ_{tm} is determined by the shear stress transport (SST) k-ω based model (Menter 1994), which combines the standard k-ϵ model (Rodi 2000) with the standard k-ω model (Wilcox 1988), by the following equation:

$$\mu_{t_m} = \frac{\left(\frac{5}{9}\right)k_m\rho_m}{\max\left(\left(\frac{5}{9}\right)\omega_m, SF_2\right)} \tag{8}$$

where ω_m is the turbulence frequency and S represents the first velocity derivative (U'). The distributions of k_m and ω_m are calculated from the following transport equations:

$$\begin{aligned}\frac{\partial(\rho_m k_m)}{\partial t} + \frac{\partial\left(\rho_m U_m^j k_m\right)}{\partial x^j} &= \frac{\partial}{\partial x^j}\left[\left(\mu_m + \frac{\mu_{t_m}}{1.18}\right)\frac{\partial k_m}{\partial x^j}\right]\\ &+ P_k - 0.09\rho_m k_m\omega_m\end{aligned} \tag{9}$$

$$\begin{aligned}\frac{\partial(\rho_m \omega_m)}{\partial t} + \frac{\partial\left(\rho_m U_m^j \omega_m\right)}{\partial x^j} &= \frac{\partial}{\partial x^j}\left[\left(\mu_m + \frac{\mu_{t_m}}{2.0}\right)\frac{\partial \omega_m}{\partial x^j}\right]\\ &+ \frac{5}{9}\frac{\omega_m}{k_m}P_k - \frac{3}{40}\rho_m\omega_m^2 + (1-F_1)\frac{2\rho_m}{1.17\omega_m}\frac{\partial k_m}{\partial x^j}\frac{\partial \omega_m}{\partial x^j}\end{aligned} \tag{10}$$

where $P_k = \mu_{t_m}S^2$ is the production term of k_m by the mean velocity gradients. F_1 and F_2 are blending functions; F_1 switches between 1 near the wall and 0 outside the boundary layer.

In the investigated settling tanks the mass and volume fraction of water are very high ($Y_w = 0.9999929626$ kg water/kg mixture and $r_w = 99.999743\%$), while the volume fractions of the solids are extremely low (ranging from 0.38×10^{-6} to 1.16×10^{-6}); then, based on Equation (3) the density of the mixture ($\rho_m = 997.004$ kg/m^3) is approximately equal to the density of water, i.e., $\rho_m \approx \rho_w = 997$ kg/m^3. Subsequently: (i) the properties of the mixture that are calculated by Equations (4)–(6) are approximately equal to the corresponding properties of the water, i.e., $U_w^i \approx U_m^i$, $\tau_m^{ij} \approx \tau_w^{ij}$ and $\tau_{Tm}^{ij} \approx \tau_{Tw}^{ij}$; (ii) the drift velocity for the water is approximately equal to zero ($U_{Dw}^i \approx 0$); (iii) the drift velocity for the solids is equal to the slip velocity, i.e., $U_{Ds,n}^i = U_{s,n}^i - U_w^i = U_{Ss,n}^i$; and (iv) the apparent diffusion stresses, which are calculated by Equation (7), are approximately equal to zero ($\tau_{Dm}^{ij} \approx 0$) and thus they are neglected in the bulk momentum Equation (2). The above-mentioned approximations justify the non-dependence of the flow field on the presence of the solids.

SS concentration field equations

The concentration field for each class of solids in the settling tanks is determined by the mass balance equation

for each class of mass fraction $Y_{n,s}$, which after using the Bussinesq approximation is written as follows:

$$\frac{\partial(\rho_m Y_{s,n})}{\partial t} + \frac{\partial\left(\rho_m Y_{s,n}\left(U_m^j + U_{Ss,n}^j\right)\right)}{\partial x^j} = \frac{\partial}{\partial x^j}\left(\mu_m \frac{\partial Y_{s,n}}{\partial x^j} + \frac{\mu_t}{0.9} m \frac{\partial Y_{s,n}}{\partial x^j}\right) \quad (11)$$

The slip velocity in Equation (11) is used to model settling in the direction of gravity of the Cartesian system and it is equal to the settling velocity $V_{s,n}$ that is determined via the following equation (Hendricks 2011):

$$U_{Ss,n} = V_{s,n} = -\frac{1,000(s-1)g\rho_w d_{n,s}^2}{18\mu_w} \quad (12)$$

where $s = 2.74$ is the specific gravity. Alternatively, the settling velocities can be determined by empirical equations based on experiments; see for example Liu & Garcia (2007) and Brennan (2001).

FTC equation

The convection-diffusion equation for the mean tracer concentration C after implementing the Bussinesq approximation has the following form:

$$\frac{\partial(\rho_w C)}{\partial t} + \frac{\partial\left(\rho_w C U_w^j\right)}{\partial x^j} = \frac{\partial}{\partial x^j}\left(\mu_w \frac{\partial C}{\partial x^j} + \frac{\mu_t}{0.9} w \frac{\partial C}{\partial x^j}\right) \quad (13)$$

The FTC is calculated from the solution of Equation (13) using the calculated steady-state flow field as input. The injection of the tracer is represented by a square step input, having duration equal to the injection time (T_{in}); see Stamou & Noutsopoulos (1994).

NUMERICAL AND CALCULATION DETAILS

Numerical code

Calculations were performed with the numerical code ANSYS-CFX (2013) that uses the finite control volume method for the spatial discretization of the domain; the equations of the model are integrated over each control volume of a co-located (non-staggered) grid layout, such that the relevant quantity (mass, momentum, C, S, k, and ω) is conserved, in a discrete sense, for each control volume. Coupling between pressure and velocity in Equations (1) and (2) is handled implicitly by a fully implicit coupled solver, which employs the 4th order accurate Rhie & Chow (1983) interpolation procedure to avoid numerical oscillations (decoupling) due to pressure checkerboard fields. Moreover, the second-order upwind Euler scheme approximates the transient term. More details can be found in ANSYS-CFX (2013).

Calculation domain and boundary conditions

The settling tanks, whose simplified top view is shown in Figure 2, are approximately symmetrical. Therefore, we decided to model the left half of the tank, which is shown in Figure 2, assuming symmetry on a plane xy in the middle of the tank. This approach has been used in cases of relatively symmetrical flows to reduce the total computational effort. An indicative top view of the calculation domain for scenario W-2B is shown in Figure 3.

We defined boundary conditions at the borders of the calculation domain. At the two inlet openings, a parallel flow was imposed with uniform horizontal velocity, vertical velocity equal to zero, and medium turbulent intensity that was set equal to 5%; the solids and tracer concentration were assumed to be uniformly distributed with concentrations equal to S_{in} and C_{in}, respectively. At the two outlet channels, the sum of flow rates was set equal to the inlet flow rate, while the gradients of C, S, k, and ω at the outlet channels were equal to zero. The vertical walls of the tank were treated as no slip – smooth wall boundaries with the exception of the right side of the tank, at which the condition of symmetry was used; see Figure 2. At the bottom of the tank, which was treated as a smooth wall, the solids were assumed to be deposited and removed from the computational domain, i.e., the formation of sludge layer was not taken into account. For scenario n-W, the free surface was treated as a free slip wall; accordingly, the normal velocity component and the normal gradients of all other variables were set equal to zero. For scenarios W, W-1B, and W-2B, the effect of wind was modeled by applying a constant horizontal flow velocity equal to 0.50 m/s on the free surface in the direction of flow (x). This value is very

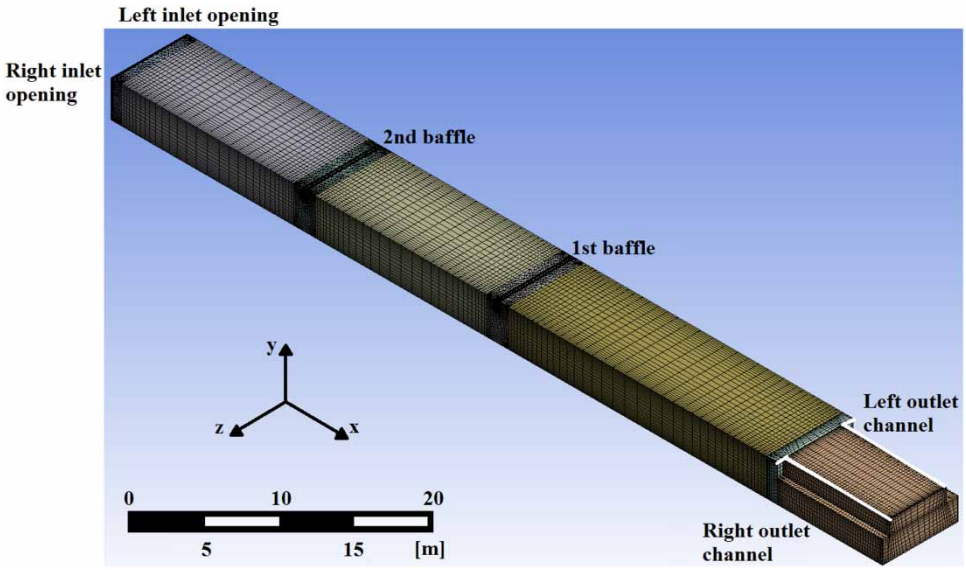

Figure 3 | View of the calculation domain for scenario W-2B.

conservative and is based on a free stream-wind speed of 15 m/s (Tsahalis 1979) which is higher than the maximum value of wind in the area of tanks that was measured in the range 7.0–9.0 m/s at a height equal to 2.0 m from the water surface.

Numerical grids

In the central part of the tank, where the geometry is simple, structured grids that employed hexahedral cells were used, while in the regions of complex geometry, such as the two inlet openings, the two outlet channels and the two baffles, unstructured grids were used; the latter permit a very accurate representation of the geometrical details in these areas, minimization of numerical errors and consistency of the solution throughout the domain. The computational grids consisted of approximately 127,000 elements for scenarios n-W and W, 181,000 elements for scenario W-1B, and 220,000 elements for scenario W-2B; these sizes were selected after a series of preliminary calculations to ensure grid independent results.

FTC calculations, processing of FTC data and hydraulic efficiency

In the FTC experiments a mass of tracer equal to $M_{in} =$ 2,250 kg was injected in the incoming flow from the two openings for a time equal to $T_{in} = 3.0$ min. The concentration of tracer was monitored at the two outlet channels, i.e., two FTCs were numerically determined for a period equal to $T_{exp} = 4T$; this duration of the numerical FTC experiments ensured that the recovery of the tracer is practically equal to 100%. The average tracer concentration in the tank was equal to $C_o = 1.23$ kg/m^3.

The calculated FTCs at the left and right outlet channels were normalized following the procedure described in Stamou & Noutsopoulos (1994), i.e., tracer concentrations (C) were divided by the average concentration (C_o), times (t) by the theoretical detention time (T), while the area below the FTC was set equal to unity (after division with tracer recovery). Then, using simple tracer mass balance the representative average FTC for the settling tank $E(\theta)$ was constructed, which represents the pdf of the normalized detention times ($\theta = t/T$) in the tank. From $E(\theta)$ the cumulative FTC $F(\theta)$ was built, whose values represent the probability that a part of the water in the tank has a detention time less or equal to t.

Certain FTC characteristics are used as indicators of the hydraulic efficiency of the tank by simply comparing their values with the corresponding values of (a) the desired ideal for settling PF and (b) the undesired completely mixed (CM) conditions. In the present work, we have estimated 15 characteristics of indicators following the

procedure and using the equations that are described in Stamou & Noutsopoulos (1994). We have grouped these indicators into four broad categories: (1) short circuiting, (2) mixing-dispersion, (3) degree of PF, and (4) efficiency. Short-circuiting indicators are the initial arrival time (θ_0) and the time at which 10% of the tracer has passed the outlet (θ_{10}). Mixing indicators are measures of the width of the FTC, such as time differences (θ_{75}–θ_{25} and θ_{90}–θ_{10}), time ratios ($M_o = \theta_{90}/\theta_{10}$) and the (statistical) variance of $E(\theta)$, *Var*. The PF indicators attempt to establish effective fractions of the PF (p) and CM conditions (1–p) regions according to the theory of Rebhun & Argaman (1965). The characteristic times, which are used as indicators of the efficiency, are the most probable time ($\theta_{\max}$) and the time at which 50% of the tracer has passed the outlet (θ_{50}).

SS calculations and removal efficiency

The SS at the inlet are usually grouped into a number of classes; in the present work we have used four classes; see the section Classes of SS. Each class has a characteristic diameter (d_s), a characteristic settling velocity (V_s), and it participates in the total mixture of solids at the inlet of the tank with a fraction or percentage (p_i). Equation (11) is solved for each class of solids to determine the steady-state concentration field for this class; then, the weighted average concentration field of the tank is determined from the concentration fields of all classes using their fractions as weights following the procedure described in Stamou *et al.* (1989).

FIELD AND LABORATORY MEASUREMENTS

Turbidity measurements at the inlet and the outlet of the tank

Turbidity measurements were carried out at the inlet and outlet of the settling tank for a period of 1 year using turbidimeters. Also, turbidity (NTU) and SS concentration (S) measurements were performed for the same influent and effluent samples according to standards methods of APHA, AWWA, and WEF (2005) to establish the following relationship:

$$S = 1.49\text{NTU} - 0.45 \tag{14}$$

Equation (14) was derived for NTU values ranging from 0.50 to 8.00 that correspond to SS concentration values from 0.30 to 11.47 mg/L and was used to translate NTU values into SS concentration values.

At the inlet, the turbidity ranged from 2.00 to 19.50 NTU and at the outlet it ranged from 0.40 to 2.50 NTU; the corresponding average daily values were equal to 5.00 and 1.60 NTU, respectively. A representative value for the SS concentration at the inlet is equal to $S_{\text{in}} = 7.0$ mg/L; for comparison purposes all calculations were reduced to this value.

Classes of SS

The SS at the inlet were grouped into four classes, C1, C2, C3, and C4 with characteristic diameters equal to 41, 17, 9.5, and 5.0 μm, respectively. The fractions of these classes were determined according to the standard methods of APHA, AWWA, and WEF (2005) equal to $p_1 = 45\%$, $p_2 = 17\%$, $p_3 = 23\%$, and $p_4 = 15\%$, respectively. The settling velocities were calculated using Equation (12) equal to 5.80, 0.96, 0.31, and 0.09 m/h, for C1, C2, C3, and C4, respectively; and the corresponding Hazen numbers ($Ha = V_s/\text{OR}$) were equal to 5.80, 0.96, 0.31, and 0.09, assuming a typical value of OR equal to 1.0 m/h.

Based on the above-mentioned values, 7.0 mg/L of SS at the inlet consist of 3.15, 1.19, 1.61, and 1.05 mg/L of classes C1, C2, C3, and C4, respectively. In the settling tank we expect: (i) 100% of the 'heavy particles', i.e., 3.15 mg/L from Class C1 ($Ha = 5.80 > > 1.0$) to settle and be completely removed from the tank; and (ii) a very large percentage (around 100%) of the 'light particles', i.e., 1.05 mg/L from Class C4 ($Ha = 0.09 < < 1.0$) not to settle and to be eventually present in the outlet. This practically implies that the removal efficiency of the tank is expected to range between 45 and 85% independently of the hydrodynamic and other processes (such as coagulation and re-suspension) in the tank. Therefore, the removal efficiency is virtually controlled by the settling behavior of the two remaining classes, C2 and C3, whose concentrations in the influent sum up to 2.80 mg/L and their

fractions add to $p_2 + p_3 = 40\%$ and whose behavior is expected to be influenced significantly by the hydrodynamics and other processes in the tank.

Distributions of the SS in the tank

We have performed a series of *in-situ* turbidity measurements along the left wall of the tank and close to it at 12 locations at $x = 0$, 5, 10, 15, 20, 25, 30, 35, 40, 45, 55, and 63 m. At each location the turbidity of the samples was measured at six water depths; then, turbidity measurements were translated to values of concentrations of SS via Equation (14). In Figure 4, two series of measurements are shown that were performed on the 3 October 2012 for OR = 1.07 m/h and on the 17 October 2012 for OR = 0.91 m/h, respectively, following the evacuation of the tanks and the removal of solids on the 28 September 2012; the first series was used for the calibration of the model and the second for its verification.

During measurements, the SS concentration at the inlet ranged between 7.50 and 7.70 mg/L. We have estimated, using the integral model CORMIX (Doneker & Jirka 2007), the average dilution of the inlet jets equal to 1.8 and 3.7 at $x = 5$ m and $x = 10$ m, respectively, and the corresponding SS concentrations equal to approximately 4.22 and 2.05 mg/L. Surprisingly, as shown in Figure 4, we have measured maximum values up to 10–12 mg/L, i.e., higher than the inlet concentrations, especially close to the inlet of the tank ($x = 0$–25 m); moreover, in this region the distribution of concentrations exhibited a relatively high degree of homogeneity. We attributed this behavior to the combination of the processes of coagulation and re-suspension in this region, which is occupied by large recirculation areas (see the section Flow field calculations); these areas are characterized by intense mixing that enhances coagulation of solids in the tank and their re-suspension from the sludge blanket that is formed near the bottom of the tank. Moreover, the day of the evacuation of the tank for the removal of sludge, we observed a small 'hill' of sludge that had formed in this region with the maximum height and length that are shown in Figure 4.

It is noted that the processes of solids accumulation, sludge-blanket formation, coagulation, and re-suspension are not described in the present model; for example, via the modification of the source terms of Equation (11) and/or the boundary condition at the bottom wall (Lyn *et al.* 1992). Nevertheless, these processes are taken into account indirectly via their effect on the distribution of solids and particularly on the change of fractions p_2 and p_3 of classes C2 and C3 that virtually control the efficiency of the tank (see the section Classes of SS); this is achieved in the process of calibration in which p_2 is determined so that the calculated removal efficiency coincides with the experimentally determined value.

RESULTS AND DISCUSSION

Flow field calculations

In Figure 5, the streamlines for all scenarios (OR = 0.85 m/h) are shown, while in Figures 6 and 7 various flow

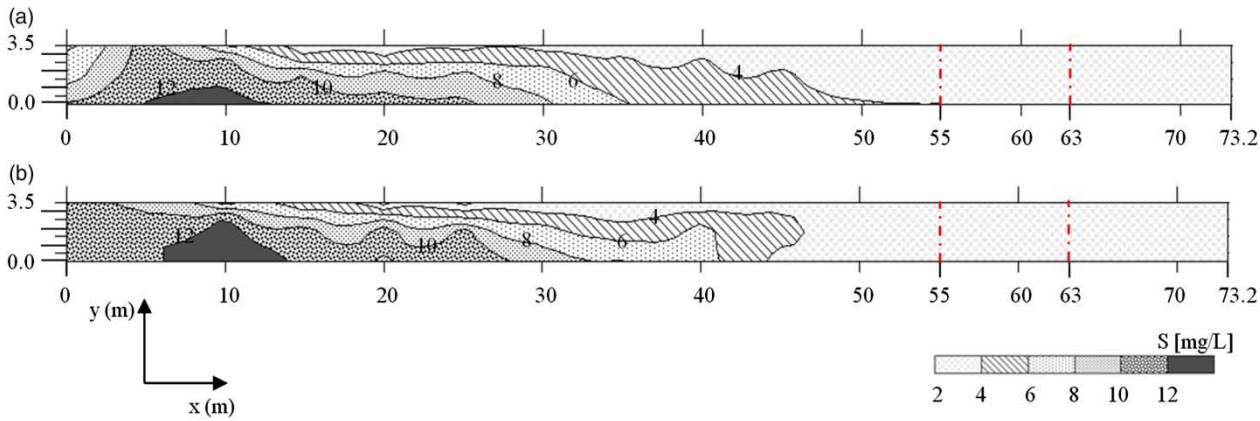

Figure 4 | Iso-concentration lines for SS in the tank based on NTU field measurements: (a) OR = 1.07 m/h and (b) OR = 0.91 m/h.

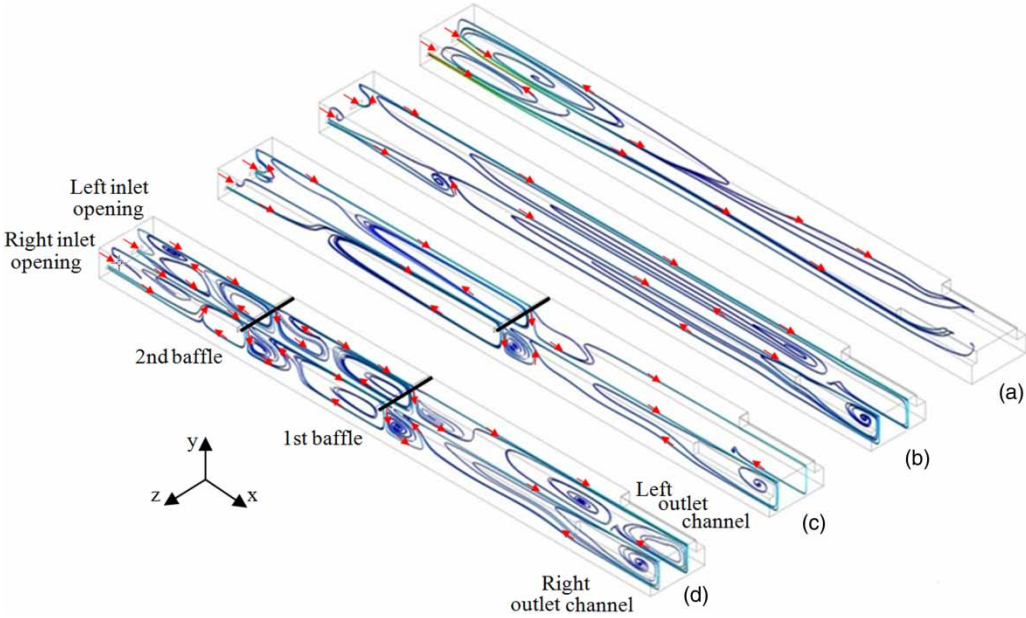

Figure 5 | Streamlines fields for scenarios: (a) n-W, (b) W, (c) W-1B, and (d) W-2B.

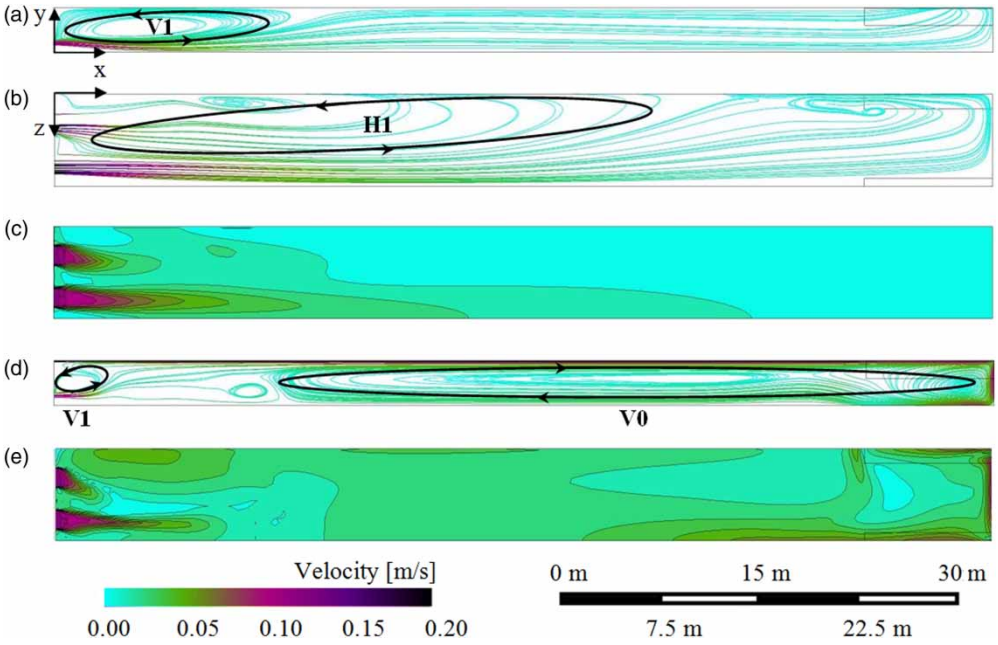

Figure 6 | Calculated flow field characteristics for scenarios n-W and W: (a) streamlines on an *xy* plane at $z = 5.3$ m for scenario n-W; (b) streamlines on an *xz* plane at $y = 0.7$ m for scenario n-W; (c) flow velocities on an *xz* plane at $y = 0.7$ m for scenario n-W; (d) streamlines on an *xy* plane at $z = 5.3$ m for scenario W; (e) flow velocities on an *xz* plane at $y = 0.7$ m for scenario W.

characteristics for the scenarios without and with baffles are shown, respectively.

Figures 5(a) and 6(a)–6(c) show that the flow field for scenario n-W is 3-D and very complex, being characterized by the formation of two main re-circulation regions (eddies). The first eddy (V1) that is shown in Figure 6(a) is created due to the incoming jets from the two inlet openings; it is anti-clockwise and its size varies along the width of the

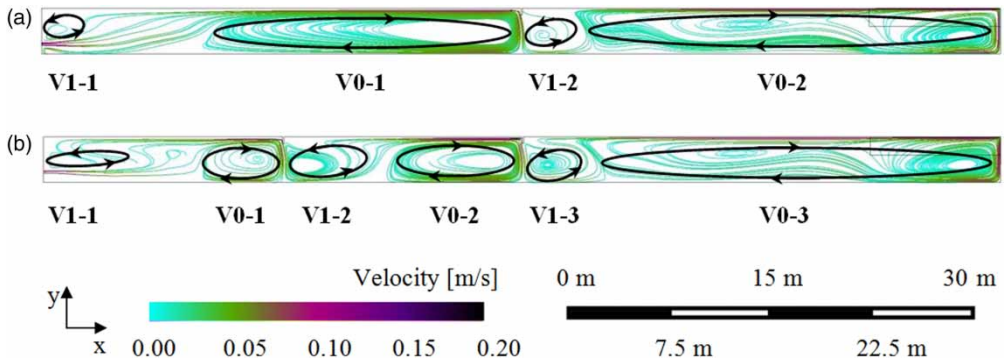

Figure 7 | Calculated streamlines on an *xy* plane at $z = 5.3$ m for scenario (a) W-1B and (b) W-2B.

tank from 20 m (close to the right, symmetry plane at $z = 7.2$ m) to 30–40 m (close to the left wall at $z = 0$ m). The second eddy (H1) that is shown in Figure 6(b) is very large and anti-clockwise; it is formed on the *xz* plane in the lower part of the tank ($y < 1.5$ m) due to the interaction of V1 with the solid wall of the tank. Flow velocities in the tank range from 0.002 to 0.02 m/s in the main body of the tank and from 0.06 to 0.08 m/s near the outlet channels (see Figure 6(c)). Moreover, the flow rates at the two outlet channels are approximately the same for all scenarios in spite of the 3-D character of flow.

Figure 6(b) and 6(c) show that the two jets entering the tank via the openings immediately undergo the influence of the two eddies (V1 and H1), which force the flow to exit the tank following short-circuiting routes; practically, H1 pushes the incoming left jet to the right and delays its appearance at the left outlet channel (see also Figure 8(a)). This short-circuiting results in much lower hydraulic

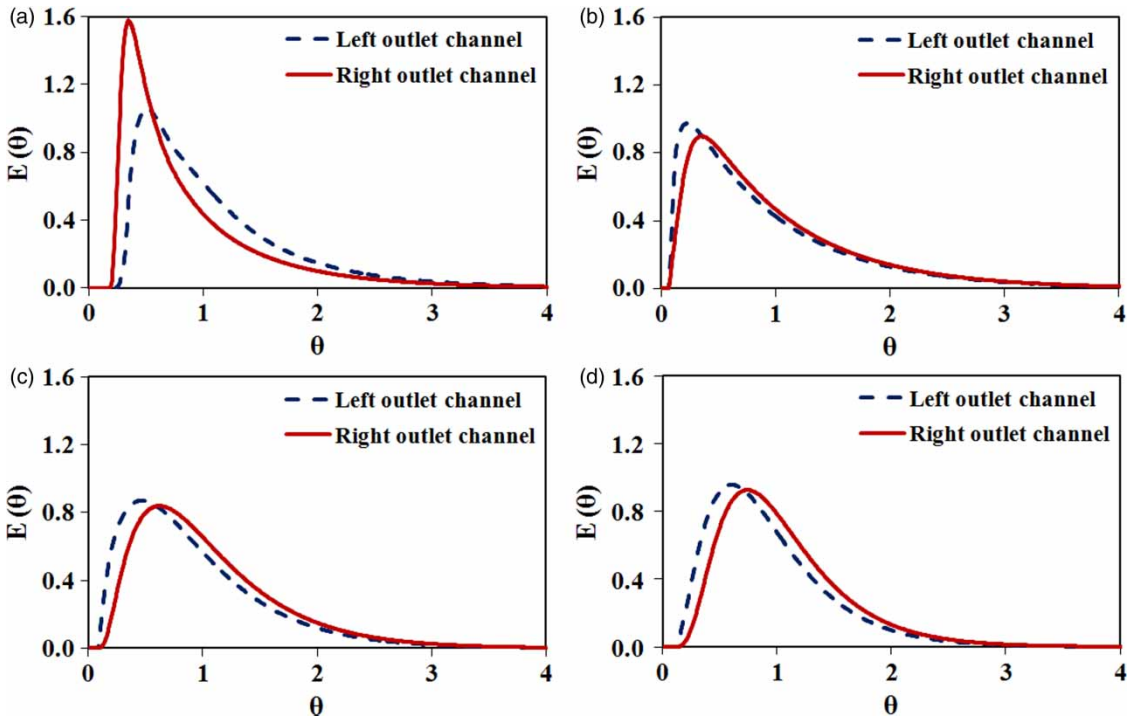

Figure 8 | Calculated FTC, $E(\theta)$, at the left and right outlet channels for scenarios (a) n-W, (b) W, (c) W-1B, and (d) W-2B.

retention times than T and reduced removal efficiencies (see also Table 1).

The degree of complexity and three-dimensionality of the flow is reduced when wind is present (see Figures 5(b) and 6(d)); the wind creates a clockwise eddy on the vertical plane xy (V0). This eddy is massive and covers approximately 70% of the tank's volume leading to intense mixing and more uniform distribution of all quantities, including velocities and SS concentrations. Moreover, it reduces the size of V1 above the inlet openings, as shown in Figure 6(d). The flow enters the tank, passes under V1, rises rapidly to the surface and exits the tank via the outlet channels following a short-circuiting path (see Figure 6(d)) with velocities that range from 0.01 to 0.10 m/s in the main body of the tank and from 0.10 to 0.14 m/s near the outlet channels (see Figure 6(e)).

Figure 7(a) shows that the use of one baffle divides the tank into two parts that occupy the first and second half of the tank, while the 2-D character of the flow that was observed in scenario W is retained. In both parts of the tank, the flow shows the behavior of scenario W with the creation of two main re-circulation regions of type V0 and V1 in each part, which are named V0-1, V1-1, and V0-2, V1-2, in the first and the second part of the tank, respectively. The flow enters the tank, passes under V1-1 and following V0-1 it raises rapidly to the surface, then it sinks to pass under the baffle that acts as a new opening for the second part of the tank, in which the same behavior of the flow is observed (see Figures 5(c) and 7(a)). Subsequently, the existence of the baffle reduces significantly the short circuiting that was observed in scenario W. Figures 5(d) and 7(b) show that the addition of the second baffle in the middle of the first half of the tank in scenario W-2B practically creates two smaller tanks in the first half of the tank and in total three smaller tanks in the whole tank; in these smaller tanks the flow is similar to that for scenario W-1B with a total of six re-circulation regions (V0-1, V1-1, V0-2, V1-2, V0-3, and V1-3), while the short circuiting is further reduced (see also Figure 8 and Table 1).

FTC calculations

In Figure 8, the calculated FTCs at the left and right outlet channel for all scenarios are shown, which correspond to the flow fields of Figure 5. These FTCs have been used to derive the average FTCs that are plotted in Figure 9(a), from which the cumulative FTCs were constructed, that

Table 1 | FTC characteristics for all scenarios

	Indicator	CM	n-W	W	W-1B	W-2B	PF
(1) Short circuiting	θ_0	0.00	0.18 (1)	0.06 (4)	0.08 (3)	0.11 (2)	1.00
	θ_{10}	0.11	0.37 (2)	0.23 (4)	0.34 (3)	0.43 (1)	1.00
	HBP	0.37	0.26 (3)	0.32 (4)	0.25 (2)	0.20 (1)	0.00
(2) Mixing-dispersion	$\theta_{75-}\theta_{25}$	1.10	0.76 (3)	0.90 (4)	0.75 (2)	0.69 (1)	0.00
	$\theta_{90}-\theta_{10}$	2.20	1.54 (3)	1.78 (4)	1.45 (2)	1.39 (1)	0.00
	M_o	21.85	5.13 (2)	8.65 (4)	5.23 (3)	4.22 (1)	1.00
	$Dt_{0.1}$	4.61	1.96 (2)	2.21 (4)	2.08 (3)	1.88 (1)	0.00
	$Dt_{0.5}$	1.39	0.76 (1)	0.97 (4)	0.91 (3)	0.89 (2)	0.00
	Var	1.00	0.13 (2)	0.19 (4)	0.13 (2)	0.10 (1)	0.00
(3) PF fractions	PFP	0.58	0.41 (2)	0.50 (4)	0.41 (2)	0.35 (1)	0.00
	SEG	0.00	0.10 (3)	0.05 (4)	0.12 (2)	0.17 (1)	0.37
	p	0.00	0.28 (3)	0.22 (4)	0.46 (1)	0.36 (2)	1.00
	$1-p$	1.00	0.72 (3)	0.78 (4)	0.54 (1)	0.64 (2)	0.00
(4) Efficiency times	$\theta_{\max}$	0.00	0.42 (3)	0.30 (4)	0.55 (2)	0.67 (1)	1.00
	θ_{50}	0.69	0.78 (3)	0.74 (4)	0.84 (2)	0.90 (1)	1.00

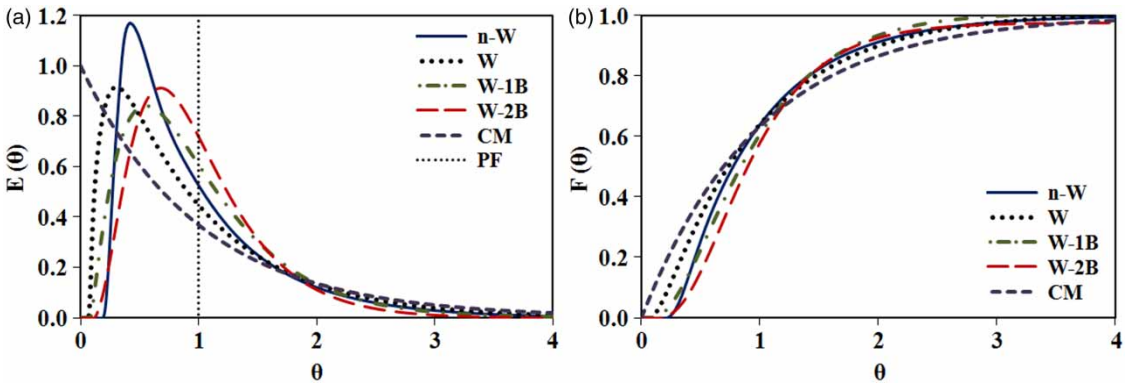

Figure 9 | Calculated FTC, $E(\theta)$, and cumulative FTC, $F(\theta)$, for all scenarios.

are shown in Figure 9(b). For comparison purposes, in both Figure 9(a) and 9(b) the theoretical curves for PF and CM conditions are also plotted, while the characteristics of all curves are depicted in Table 1. The numbers in parentheses in Table 1 compare the four scenarios; (1) refers to the best scenario and (4) to the worst.

All FTCs in Figures 8 and 9(a) consist of three parts: the first rising part embodies the volume of tracer leaving the tank via a short-circuiting path; the second declining part represents the volume of tracer, which exits the tank after following a series of paths imposed by the flow fields of Figure 5; and the third part is the 'tail' of the FTC, which represents the volume of tracer that exits the tank after remaining in the relatively slow (re-circulation) regions in the tank.

Figure 8(a) shows that for scenario n-W, the tracer arrives earlier at the right outlet channel than at the left (smaller values of initial arrival times), after having undergone relatively smaller levels of mixing that are indicated by the relatively high values of maximum concentration. This behavior is consistent with the 3-D flow field (see the section Flow field calculations), but it is contrary to the expected behavior for 2-D flows in which the tracer arrives earlier at the left outlet channel (due to the larger size of eddy V1 that is equal to approximately 35 m) than at the right outlet channel (where the size of V1 is equal to approximately 20 m). Practically, this means that in tanks where the flow is expected to be 3-D and with more than one outlet channel, the experimental derivation of just one FTC at one of the outlet channels is not necessarily representative. For scenarios W, W-1B, and W-2B there are no significant differences between the FTCs at the left and right outlet channels due to the relatively 2-D character of the flow imposed by the action of the wind in the x-direction. Moreover, for all scenarios, the total mass of tracer at the two outlet channels was approximately the same, following the equal distribution of flow rates (see the section Flow field calculations); this behavior was also valid for scenario n-W in spite of the significant differences in the shapes of FTC.

The FTC characteristics of the initial geometry (scenario n-W) shown in Table 1 indicate: (1) high short-circuiting (low values of $\theta_0 = 0.18$ and $\theta_{10} = 0.37$); (2) intense mixing (high values of mixing indicators); (3) low fraction of PF ($p = 28\%$); and (4) low efficiency (low values of $\theta_{max} = 0.42$ and $\theta_{50} = 0.78$).

Based on Figure 9 and the characteristics of Table 1, scenario W exhibits the worst behavior (noted also in Table 1 with the number 4 in parentheses for all characteristics), i.e., it shows very high levels of short circuiting (extremely low values of $\theta_0 = 0.06$ and $\theta_{10} = 0.23$), very intense mixing (very high values of mixing indicators), very low fraction of PF ($p = 22\%$) and very low efficiency (very low values of $\theta_{max} = 0.30$ and $\theta_{50} = 0.74$). Scenario W-2B with two baffles exhibits the best hydraulic performance (noted also in Table 1 with the number 1 in parentheses for the majority of the characteristics), while scenario W-1B with one baffle seems to approach more PF conditions than scenario n-W (with no wind), which however exhibits the lowest degree of mixing, judging only by the maximum concentration (see Figure 9(a)). The above-mentioned behavior is in accordance with the theoretical concept that the flow in a series of CM reactors approaches

PF with increasing number of reactors, but also with the flow calculations for all scenarios in which we have observed the formation of 4 and 6 recirculation regions for scenarios W-1B and W-2B, respectively.

Calculations of the concentrations of SS

Calibration and verification of the model

We performed the calibration of the model for the first series of measurements (see the section Distributions of the SS in the tank) and determined the percentage of the second class of SS equal to $p_2 = 36\%$ for which the calculated removal efficiency coincides with the experimentally determined value. Moreover, the calculated SS concentrations at $x = 55$ m and $x = 63$ m that are plotted in Figure 10(a) show very good agreement with measurements. To verify the model, we used the determined value of p_2 and performed calculations for the second series of measurements. The removal efficiency was calculated equal to 70.86%, i.e., it is the same as the experimentally determined value, while the comparison of calculated SS concentrations with measurements, which is shown in Figure 10(b), is also very satisfactory, thus indicating that the verification of the model is successful. The main data of the processes of calibration and verification are shown in Table 2 together with the maximum removal efficiencies assuming ideal settling in PF conditions, which were calculated equal to 79.75 and 83.88% for OR = 1.07 and 0.91 m/h, respectively; i.e., they were by 13% higher than the actual values.

From the data of Table 2 some important practical conclusions can be drawn. First, the concentrations of solids in the influent for the classes C1, C2, C3, and C4 are 3.15, 2.52, 0.28, and 1.05 mg/L, respectively. From the total of 7.0 mg/L it is expected that 3.15 mg/L (100% of class C1) is completely removed, while 1.05 mg/L (100% of class C4) is always present in the outlet, i.e., the maximum removal efficiency of the tank can never exceed 85%, which is indeed correct (see the section Classes of SS).

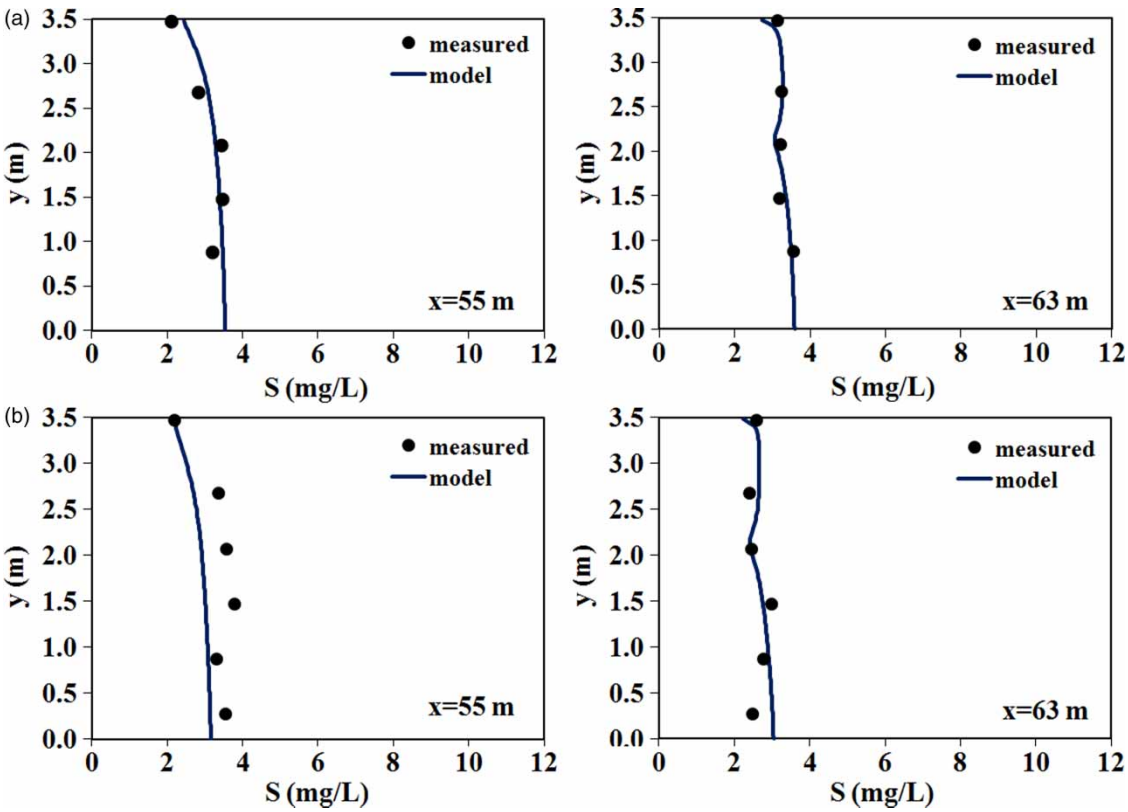

Figure 10 | Calculated SS concentrations vs. measurements: (a) OR = 1.07 m/h, (b) OR = 0.91 m/h.

Table 2 | Summary of the calculations for the calibration and verification of the model

Characteristics at inlet				Calibration for OR = 1.07 m/h			Verification for OR = 0.91 m/h		
Class	p_i (%)	V_s (m/h)	S_{in} (mg/L)	S_{out} (mg/L)	R (%)	R (ideal settling) (%)	S_{out} (mg/L)	R (%)	R (ideal settling) (%)
C1	45	5.80	3.15	0.03	99.00	100.00	0.01	99.71	100.00
C2	36	0.96	2.52	1.08	57.02	89.65	0.88	64.96	100.00
C3	4	0.31	0.28	0.21	24.93	28.84	0.20	28.35	33.53
C4	15	0.09	1.05	0.96	8.69	8.81	0.95	9.96	10.24
Total	100	–	7.00	2.28	67.43	79.75	2.04	70.86	83.88

Second, the actual removal efficiency of the tank depends mainly on the fractions of classes C2 and C3, whose concentrations in the influent sum up to 2.8 mg/L; this remark virtually justifies the selection of p_2 of class C2 as 'calibrated parameter' ($p_3 = 40\% - p_2$). Assuming a conservative percentage of removal for these fractions equal to 30%, the minimum removal efficiency of the tank is expected to be higher than 57%.

Distributions of SS

The steady-state SS concentration fields are plotted in Figure 11 and the removal efficiencies for all classes and scenarios are shown in Table 3. As in Table 1, the numbers in parentheses compare the four scenarios: (1) refers to the best scenario and (4) to the worst. Figure 11 shows that the concentration fields are strongly influenced by the respective flow fields, which are shown in Figure 5; in the recirculation areas SS concentrations tend to be uniformly distributed, while the lowest values are observed close to the free surface and the highest near the bottom due to the process of settling. Figure 11 shows that the action of wind (scenario W) leads to higher values of SS concentration in the tank compared to the no-wind scenario (n-W); the iso-concentration lines of SS are shifted to the right, i.e., the solids move faster toward the outlet due to the action of wind on the water surface, and the vertical distribution of SS concentration is relatively more uniform, since mixing

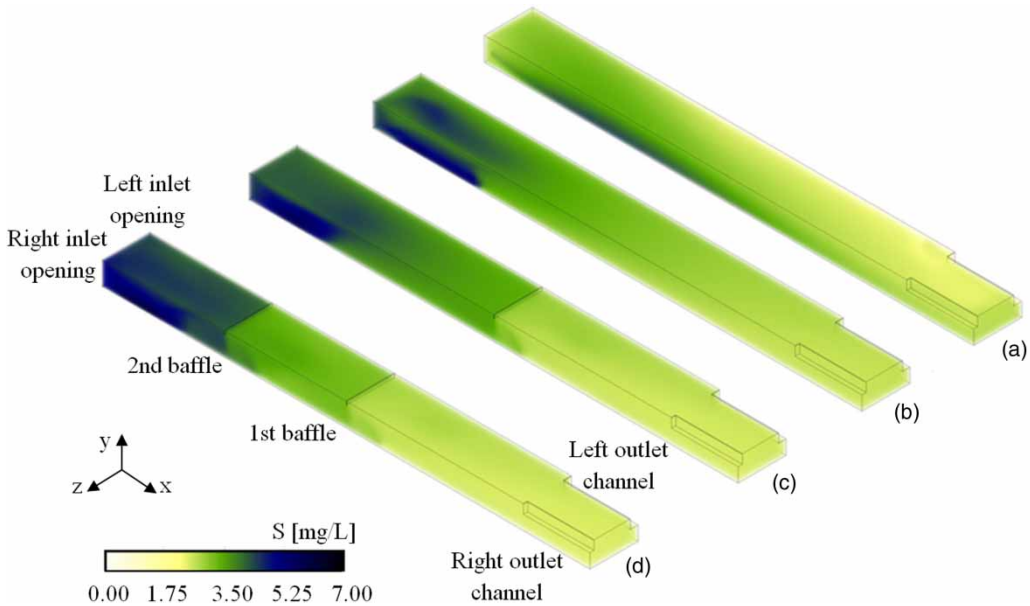

Figure 11 | Concentration fields of SS for scenarios (a) n-W, (b) W, (c) W-1B, and (d) W-2B.

Table 3 | Removal efficiencies (%) for all scenarios and ideal settling (OR = 0.85 m/h)

Scenario	n-W	W	W-1B	W-2B	Ideal settling (PF)
Class					
C1	100.00 (1)	97.90 (4)	99.09 (3)	99.61 (2)	100.00
C2	68.36 (1)	59.09 (4)	62.81 (3)	64.95 (2)	100.00
C3	29.81 (1)	28.13 (4)	29.04 (3)	29.65 (2)	36.05
C4	10.51 (1)	10.16 (4)	10.23 (3)	10.36 (2)	11.01
Total	72.48 (1)	68.07 (4)	70.00 (3)	71.04 (2)	84.18

is intense in the large wind-generated re-circulation area V0 (see Figure 6(d)). The use of one baffle in scenario W-1B divides the settling tank into two parts and practically shifts the iso-concentration lines of SS upstream thus improving the efficiency of the tank, while the implementation of two baffles divides the tank into three parts and improves further its efficiency.

Removal efficiency, its relation with hydraulic efficiency and practical aspects

According to Table 3, the tank shows the best removal efficiency (72.48%) without wind (scenario n-W), which as expected is significantly lower than the efficiency for ideal settling (84.18%). When the wind is present (scenario W), the worst efficiency (68.07%) is observed, which however increases using one baffle (70.00%, for scenario W-1B), while a further improvement can be achieved when two baffles are installed in the tank (71.04%, for scenario W-2B). This order of removal efficiency, which was observed among the four scenarios for the average SS concentrations, was also valid separately for each class of solids.

The order of removal efficiency among the four scenarios shown in Table 3 is not the same as that of hydraulic efficiency of Table 1, in which the scenarios with baffles under wind conditions (scenarios W-1B and W-2B) showed a better efficiency than the scenario without wind (scenario n-W) (see the section FTC calculations). In other words, in the comparison of various alternative scenarios for tank configuration or operation, the scenario that shows the best hydraulic performance does not necessarily exhibit the best removal efficiency. The main reason for this behavior is that the removal efficiency is dependent upon the characteristics of SS in the effluent, while the hydraulic efficiency is not. Therefore, when the influent contains mainly very heavy or very light particles (i.e., particles with very high or very low Hazen numbers), the hydrodynamics in the tank does not affect its removal efficiency significantly, because it is expected that the very heavy particles are removed by 100%, while the very light particles are not removed at all.

Table 3 shows that for windy conditions the SS concentration in the effluent increases from 1.93 to 2.24 mg/L, i.e., the difference is not that pronounced. In other words, the effect of the wind on the effluent concentration is not intense, as it was initially considered based on the optical observations during strong winds (extended areas with high turbidity, especially close to the inlet of the tank), and even more, as it was expected based on the dramatic differences of the calculated flow fields. The presence of turbid areas is due mainly to the re-suspension of the solids, which are accumulated in the bottom of the tank. The extent of these areas and the degree of turbidity are expected to decrease significantly when the sludge removal mechanism is set back in operation. Under these normal conditions and during strong winds, the use of one or two baffles improves the efficiency of the tank by reducing the SS concentrations at the effluent to 2.10 and 2.03 mg/L, respectively.

CONCLUSIONS

We applied a CFD model (i) to investigate the expected negative effect of the wind on the hydrodynamic and settling performance of the settling tanks of the WTP of Aharnes, and (ii) to evaluate the improvement resulting from the installation of one and two baffles in the tank. The wind was modeled using a simple, but very conservative approach, which involves the setting of a constant horizontal flow velocity on the free surface. We calibrated and verified the part of the model that describes the behavior of SS with field measurements; in this validation procedure the effects of solids re-suspension and coagulation, which were not accounted by the model explicitly, were indirectly taken into account.

Calculations showed that the effect of wind on the flow field and the hydraulic efficiency is very strong, with the creation of massive re-circulation areas with intense mixing and high short circuiting. However, the effect of wind on the settling performance of the tanks was not pronounced; their initial removal efficiency of 72.48% was reduced to 68.07%, when a strong wind was present. Moreover, it was increased to 70.00 and 71.04%, when one or two baffles were installed, respectively.

ACKNOWLEDGEMENTS

The present work was performed in the NTUA within the framework of the research project entitled 'Improving the efficiency of settling tanks of the WTP of EYDAP SA in Aharnes using mathematical models'. The financial support provided by EYDAP SA is gratefully acknowledged. Furthermore, the authors would like to thank the personnel of EYDAP SA for the useful discussions and for providing the required information and data, especially Mr S. Georgiadis, Mrs M. Xanthaki, Mrs R. Polomarkaki, Mr G. Dimtsas, and Mrs M. Spanakou.

REFERENCES

Alliet-Gaubert, M., Sardeing, R., Xuereb, C., Hobbes, P., Letellier, B. & Swaels, P. 2006 CFD Analysis of industrial multi-staged stirred vessels. *Chem. Eng. Process. Process Intensif.* **45** (5), 415–427.

ANSYS-CFX, Release 14.0. Available at: http://www.ANSYS.com (accessed 10 March 2013).

Asgharzadeh, H., Firoozabadi, B. & Afshin, H. 2012 Experimental and numerical simulation of the effect of particles on flow structures in secondary sedimentation tanks. *J. Appl. Fluid Mech.* **5** (2), 15–23.

Brennan, D. 2001 *The numerical simulation of two-phase flows in settling tanks*. PhD thesis, Imperial College of Science, Technology and Medicine of the University of London.

Bridgeman, J., Jefferson, B. & Parsons, S. A. 2010 The development and application of CFD models for water treatment flocculators. *Adv. Eng. Softw.* **41** (1), 99–109.

Camp, T. R. 1946 Sedimentation and the design of settling tanks. *Trans. ASCE* **111** (2285), 895–936.

Doneker, R. L. & Jirka, G. H. 2007 *CORMIX User Manual: A Hydrodynamic Mixing Zone Model and Decision Support System for Pollutant Discharges into Surface Waters*. EPA-823-K-07-001.

Dufresne, M., Vazquez, J., Terfous, A., Ghenaim, A. & Poulet, J.-B. 2009 Experimental investigation and CFD modelling of flow, sedimentation and solids separation in a combined sewer detention tank. *Comput. Fluids* **38** (5), 1042–1049.

Egorov, Y., Menter, F., Klöker, M. & Kenig, E. Y. 2005 On the combination of CFD and rate-based modelling in the simulation of reactive separation processes. *Chem. Eng. Process. Process Intensif.* **44** (6), 631–644.

Falconer, R. A. & Liu, S. Q. 1987 Mathematical model study of plug flow in a chlorine contact tank. *Water Environ. J.* **1** (3), 279–290.

Ghidossi, R., Veyret, D. & Moulin, P. 2006 Computational fluid dynamics applied to membranes: state of the art and opportunities. *Chem. Eng. Process. Process Intensif.* **45** (6), 437–454.

Goula, A. M., Kostoglou, M., Karapantsios, T. D. & Zouboulis, A. I. 2008 A CFD methodology for the design of sedimentation tanks in potable water treatment – case study: the influence of a feed flow control baffle. *Chem. Eng. J.* **140** (1–3), 110–121.

Hazen, A. 1904 On sedimentation. *Trans. ASCE* **53** (980), 45–88.

Hendricks, D. 2011 *Fundamentals of Water Treatment Unit Processes: Physical, Chemical and Biological*. CRC Press, Boca Raton, FL, USA.

Ishii, M. 1975 Thermo-fluid dynamic theory of two-phase flow. Collection de la Direction des Etudes et Researches de EDF, Eyrolles, 22, Paris, France.

Khezri, S. M., Biati, A. & Erfani, Z. 2012 Determination of the effect of wind velocity and direction changes on turbidity removal in rectangular sedimentation tanks. *Water Sci. Technol.* **66** (12), 2814–2820.

Liu, X. & Garcia, M. H. 2007 Numerical Modeling of the Calumet Water Reclamation Plant (CWRP) Primary Settling Tanks, Civil Engineering Studies, Hydraulic Engineering Series No 80. Department of Civil and Environmental Engineering, University of Illinois at Urbana-Champaign, IL, USA.

Lyn, D. A., Stamou, A. I. & Rodi, W. 1992 Density currents and shear induced flocculation in sedimentation tanks. *J. Hydraul. Eng.* **118** (6), 849–867.

Matko, T., Fawcett, N., Sharp, A. & Stephenson, T. 1996 Recent progress in the numerical modelling of wastewater sedimentation tanks. *Process Saf. Environ. Prot.* **74** (4), 245–258.

Menter, F. R. 1994 Two-equation eddy-viscosity turbulence models for engineering applications. *AIAA J.* **32** (8), 1598–1605.

Okoth, G., Centikaya, S., Bruggermann, J. & Thoming, J. 2008 On hydrodynamic optimization of multi-channel counter-flow lamella settlers and separation efficiency of cohesive particles. *Chem. Eng. Process. Process Intensif.* **47** (1), 90–100.

Rebhun, M. & Argaman, Y. 1965 Evaluation of hydraulic efficiency of sedimentation basins. *J. Sanit. Eng. Div.* **91** (5), 37–48.

Rhie, C. M. & Chow, W. L. 1983 Numerical study of the turbulent flow past an airfoil with trailing edge separation. *AIAA J.* **21**, 1527–1532.

Rodi, W. 2000 *Turbulence Models and Their Application in Hydraulics – A State of the Art Review*. 3rd edn. IAHR, the Netherlands.

Shiono, K. & Teixeira, E. C. 2000 Turbulent characteristics in a baffled contact tank. *J. Hydraul. Res.* **38** (6), 403–416.

Sivakumar, M. & Lowe, S. A. 1990 Simulation of the effect of wind on rectangular sedimentation tanks. In: *Conference on Hydraulics in Civil Engineering, Sydney, Australia*, pp. 74–78.

Souadnia, A., Soltana, F., Lesage, F. & Latifi, M. A. 2005 Some computational aspects in the simulation of hydrodynamics in a trickle-bed reactor. *Chem. Eng. Process. Process Intensif.* **44** (8), 847–854.

Stamou, A. I. 1993 Prediction of hydrodynamic characteristics of oxidation ditches using the k-epsilon turbulence model, Engineering Turbulence Modelling and Experiments: 2. In: *Proceedings of the 2nd International Symposium*, Florence, Italy, pp. 261–272.

Stamou, A. I. 2002 Verification and application of a mathematical model for the assessment of the effect of guiding walls on the hydraulic efficiency of chlorination tanks. *J. Hydroinform.* **4**, 245–254.

Stamou, A. I. 2007 Discussion of two-dimensional simulation model of sediment removal and flow in rectangular sedimentation basin. *J. Environ. Eng.* **133** (9), 944–945.

Stamou, A. I. & Noutsopoulos, G. 1994 Evaluating the effect of inlet arrangement in settling tanks using the hydraulic efficiency diagram. *Water SA* **20** (1), 77–83.

Stamou, A. I., Adams, E. W. & Rodi, W. 1989 Numerical modeling of flow and settling in primary rectangular clarifiers. *J. Hydraul. Res.* **27** (5), 665–682.

Stamou, A. I., Latsa, M. & Assimacopoulos, D. 2000 Design of two-storey final settling tanks using mathematical models. *J. Hydroinform.* **2** (4), 235–245.

Stamou, A. I., Theodoridis, G. & Xanthopoulos, K. 2009 Design of secondary settling tanks using a CFD model. *J. Environ. Eng.* **135** (7), 551–561.

Standard Methods for the Examination of Water and Wastewater 2005 21st edn. American Public Health Association/ American Water Works Association/Water Environment Federation, Washington DC, USA.

Tsahalis, D. T. 1979 Theoretical and experimental study of wind and wave induced drift. *J. Phys. Oceanogr.* **9** (6), 1243–1257.

Wilcox, D. C. 1988 Reassessment of the scale determining equation for advanced turbulence models. *AIAA J.* **26** (11), 1299–1310.

First received 26 June 2014; accepted in revised form 4 February 2015. Available online 6 March 2015